Available online at www.sciencedirect.com
ScienceDirect
Thin-Walled Structures 45 (2007) 620–633
THIN-WALLED STRUCTURES
www.elsevier.com/locate/tws

Semi-analytical postbuckling and strength analysis of arbitrarily stiffened plates in local and global bending

Lars Brubak, Jostein Hellesland*

Mechanics Division, Department of Mathematics, University of Oslo, NO-0316 Oslo, Norway

Received 20 October 2006; accepted 16 April 2007
Available online 12 July 2007

Abstract

A semi-analytical method for pre- and postbuckling analysis of imperfect plates with arbitrary stiffener arrangements, subjected to in-plane biaxial and shear loading, is presented. By using large deflection theory in combination with the Rayleigh–Ritz approach on an incremental form, the method is able to trace both local and global equilibrium paths. Ultimate strength predictions are made using the von Mises' yield criterion applied to the membrane stresses as collapse criterion. A Fortran computer program based on the presented theory is developed and computed results are verified by comparisons with nonlinear finite element analysis. Relatively high numerical accuracy is achieved with small computational efforts. The method is therefore suited also for design optimisation and reliability studies.

Keywords: Stiffened plates; Arbitrary stiffener arrangement; Ultimate strength; Semi-analytical method; Large deflection theory; Local–global bending interaction; Buckling; Postbuckling; Rayleigh–Ritz method

1. Introduction

The traditional design approach of stiffened plates in ships, offshore installations, steel bridges, aircrafts, etc., is to use explicit design formulas [1–3]. These are limited to regularly stiffened plates. For more complex plate geometries and stiffener arrangements, other methods must be applied. Finite element analysis, involving model generation, numerical computation and postprocessing, will normally be very time consuming. Computational methods using a semi-analytical approach for buckling and strength analysis of stiffened plates are becoming more common, not least due to their computational efficiency and user-friendliness.

A semi-analytical method for analysis of buckling and strength of plates with arbitrary stiffener arrangement is presented in Brubak et al. [4] for constant thickness plates, and in Brubak and Hellesland [5] for plates with varying, stepwise constant thickness. These studies make use of a displacement magnifier approach involving the eigenvalue and eigenmode calculated using small deflection theory, and finally stress computations using large deflection theory. This displacement magnifier approach implies that it is not capable of predicting the reserve strength beyond the elastic buckling load. Although neglecting the reserve strength may be a sound design approach in practical cases where the structural elements are not allowed to buckle elastically, it is still of interest to be able to trace the nonlinear postbuckling behaviour beyond the elastic buckling load.

For such tracing, more advanced semi-analytical methods using large deflection theory for both the displacements and the stress calculations can be applied. For regularly stiffened plates, a usual approach is to consider a model consisting of a plate field with only one or two stiffeners included. Such an approach for local bending has been presented by Byklum and Amdahl [6]. In Byklum et al. [7], it has been shown that such local pre- and postbuckling analysis may be used to provide anisotropic stiffness coefficients that may be used in an orthotropic plate theory to analyse the global buckling and postbuckling response of stiffened plates. In such formulations, it is not possible to analyse a plate provided with stiffeners of different profiles, unequal stiffener spacing or linear varying applied stress in the direction of the stiffeners,

*Corresponding author.
E-mail address: josteinh@math.uio.no (J. Hellesland).

0263-8231/$ - see front matter
doi:10.1016/j.tws.2007.04.011

etc. In other approaches, the entire stiffened plate field is included. Such an approach has been presented by Paik and Lee [8]. In that work, involving regular stiffeners modelled by beams, the stiffener model is not able to capture an asymmetric bending behaviour. A review of additional semi-analytical methods is given in Brubak et al. [4].

The semi-analytical methods for nonlinear postbuckling analysis mentioned above are restricted to regular stiffeners. In the present work, the main objective has been to present a semi-analytical, large deflection theory model for biaxially and shear loaded (in-plane) plates with regular or irregular stiffeners. The model should be able to capture the interaction between local and global plate bending, and be able to trace the pre- and postbuckling response including asymmetric effects, and to predict the reserve strength beyond the elastic buckling load. It is based on an incremental form of the Rayleigh–Ritz method and follows the general solution strategy outlined by Steen [9] and Byklum et al. [6]. The entire stiffened plate field is modelled, and thus the present model does not have the same restrictions as that of models with only one or two stiffeners and a segment of the plate field included in the model formulation. On the other hand, the present stiffener modelling is simplified and is not capable of predicting local failure modes of the stiffeners, which, consequently, must be designed such that they do no buckle prematurely. The plates may have regular or arbitrarily spaced and oriented stiffeners, and they may have various restraints at plate edges and in the interior of the plate. Arbitrary stiffeners may be real or they may be included to enclose complex plate geometries, such as triangular, trapezoidal and other plate shapes.

2. Plate definition and boundary conditions

A stiffened plate is usually a part of a larger structure surrounded by adjacent girders and plates, and its boundaries are typically supported with strong longitudinal and transverse girders or strong flanges preventing out-of-plane displacements. In some cases, for example in the stern or in the bow of a ship, the stiffener arrangement may be irregular. For such plates and for girder webs, the stiffeners are often sniped at their ends, and thus not subjected to any external loads at their ends. In a case with regular stiffeners, the stiffeners are often attached to the surrounding structure which will impose in-plane stresses at stiffener ends (continuous stiffeners).

The model formulations are derived by considering the plate in Fig. 1(a). The number of stiffeners may be arbitrary and the cross-section profiles may by eccentric as in Fig. 1(b), or symmetric about the middle plane of the plate. In the figure, a typical open stiffener profile is shown, but the stiffener profile can also be closed. The plate is provided with supports preventing out-of-plane displacements along all the outer boundaries, and the edges are forced to remain straight, but free to move in the in-plane directions. A boundary or a part of a boundary may be simply supported, clamped or something in between. In addition to the stiffeners, translational and rotational springs can be added along arbitrary oriented lines, in order to model restraints by a surrounding structure at the edges or in the interior of the plate.

The loading may consist of a combination of in-plane shear stress and linear varying in-plane compression or tension stress. Positive directions are shown in Fig. 1(a). The total stress along the plate edges are those shown in Fig. 1(a) plus those required to maintain straight edges. The latter stresses are obtained from the present analysis, and their resultant over the length of an edge is zero.

The stiffeners are modelled as beams with out-of-plane bending stiffness only. The method can therefore not predict local stiffener failure modes (including lateral torsional buckling). This may not imply any severe limitation in practical design as given constructional stiffener requirements and design rules normally prevent local instabilities of stiffeners. Further, in a design situation, the stiffeners are usually dimensioned to be sufficiently strong such as to prevent global bending behaviour. In such cases, the stiffeners will not be subjected to additional stress due to global bending, and local instabilities of stiffeners are even more unlikely.

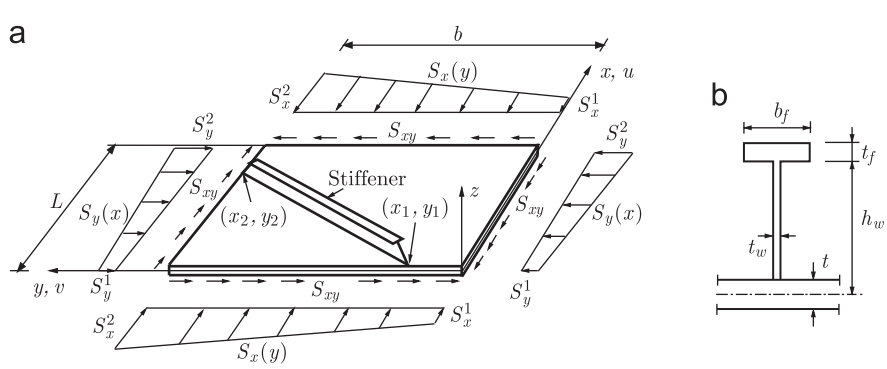

Fig. 1. (a) Stiffened plate subjected to in-plane shear stress and in-plane, linear varying compression or tension stress, and (b) cross-section of an eccentric stiffener.

3. Material, kinematics and equilibrium

The material is assumed to be linearly elastic with Young's modulus E and Poisson's ratio ν. Normal stresses and strains are defined to be positive in tension, i.e., opposite to the definition of applied normal stresses in Fig. 1(a). Positive definition of shear stresses is the same as of S_{xy} in the figure.

In the postbuckling range, out-of-plane displacements (deflections) may become significant compared to the plate thickness. To be able to predict such displacements and resulting stress redistributions with sufficient accuracy, the basic premises for the conventional nonlinear plate theory for large deflections, or rather moderately large deflections [10], or theory for intermediate class of deformations [11], is adopted. It is based on the assumptions of small in-plane strains and large rotations at the middle plane (i.e., for membrane strains). Further, for the additional bending strain, small rotations are assumed such that linearised curvature expressions can be used. The theory further implies Kirchhoff's two classical thin plate assumptions that (1) normals to the middle plane remain normal to the deflected middle plane, and that (2) normal stresses in the transverse direction are negligible. The first of these assumptions leads to bending strains that vary linearly (with z) across the plate thickness, and the second allows for the use of Hooke's law for plane stress. For the stiffeners (beams), comparable beam assumptions ("plane sections remain plane" and Hooke's law for uniaxial stress) are adopted.

The total in-plane normal strain (ε) and shear strain (γ) in a material point can now be defined by

$$\varepsilon_x = \varepsilon_x^m - zw_{,xx}, \quad \varepsilon_y = \varepsilon_y^m - zw_{,yy}, \tag{1}$$

$$\gamma_{xy} = \gamma_{xy}^m - 2zw_{,xy}, \tag{2}$$

where the first terms are membrane strains and the second terms are the bending strains. For a plate with an initial out-of-plane imperfection w_0 and additional out-of-plane displacement w, the membrane strains become [12]

$$\varepsilon_x^m = u_{,x} + \tfrac{1}{2}w_{,x}^2 + w_{0,x}w_{,x}, \tag{3}$$

$$\varepsilon_y^m = v_{,y} + \tfrac{1}{2}w_{,y}^2 + w_{0,y}w_{,y}, \tag{4}$$

$$\gamma_{xy}^m = u_{,y} + v_{,x} + w_{,x}w_{,y} + w_{0,x}w_{,y} + w_{0,y}w_{,x}, \tag{5}$$

where u and v are the displacements of the middle plane of the plate in the x- and y-direction, respectively. Subscripts preceded by a comma are used in normal fashion to denote partial derivatives ($w_{,x} = \partial w/\partial x, w_{,xx} = \partial^2 w/\partial x^2$, etc.).

In-plane stresses are expressed through Airy's stress function $F(x,y)$, defined by $\sigma_x^m = F_{,yy}$, $\sigma_y^m = F_{,xx}$ and $\tau_{xy}^m = -F_{,xy}$. By differentiation and combination of Eqs. (3)–(5), a compatibility equation for the in-plane strains can be derived. By substituting strains from Hooke's law for plane stress and Airy's stress function into this equation, the following nonlinear plate compatibility equation [12] is obtained:

$$\nabla^4 F = E(w_{,xy}^2 - w_{,xx}w_{,yy} + 2w_{0,xy}w_{,xy} - w_{0,xx}w_{,yy} - w_{0,yy}w_{,xx}). \tag{6}$$

The in-plane equilibrium of the plate is identically satisfied by the use of Airy's stress function. The out-of-plane equilibrium will be satisfied using the principle of stationary potential energy (Rayleigh–Ritz method).

4. Model discretisation

A set of continuous functions defined by

$$w_0(x,y) = \sum_{i=1}^{M}\sum_{j=1}^{N} b_{ij}\sin\left(\frac{\pi i x}{L}\right)\sin\left(\frac{\pi j y}{b}\right), \tag{7}$$

$$w(x,y) = \sum_{i=1}^{M}\sum_{j=1}^{N} a_{ij}\sin\left(\frac{\pi i x}{L}\right)\sin\left(\frac{\pi j y}{b}\right) \tag{8}$$

are assumed for the initial out-of-plane displacement imperfection (w_0) and the additional out-of-plane displacements (w), respectively (positive upwards in Fig. 1). Here, a_{ij} are the unknown out-of-plane displacement amplitudes, b_{ij} are known imperfection amplitudes, L is the plate length (in the x-direction) and b the plate width (in the y-direction).

Although each component in a series of sine functions represents a simply supported condition, added together they are nearly able to describe also a clamped, or partially restrained, condition. The assumed displacement field is therefore able to handle plates with rotational various boundary conditions along the edges.

The well known solution of Eq. (6) proposed by Levy [13] is assumed. With the assumed displacement field, it can be given on the form

$$F(x,y) = F^L + F^{NL}, \tag{9}$$

where the terms

$$F^L = -S_x^1\frac{y^2}{2} - (S_x^1 - S_x^2)\frac{y^3}{6b} - S_y^1\frac{x^2}{2} - (S_y^1 - S_y^2)\frac{x^2}{6L} - S_{xy}xy, \tag{10}$$

$$F^{NL} = \sum_{i=0}^{2M}\sum_{j=0}^{2N} f_{ij}\cos\left(\frac{i\pi}{L}x\right)\cos\left(\frac{j\pi}{b}y\right) \tag{11}$$

represent a linear and a nonlinear stress variation over the plate surface, respectively. Here, the coefficients f_{ij} are functions of the amplitudes of w and w_0. External stresses (S_x^1, etc.) are defined in Fig. 1.

The first term (F^L) represents the applied edge stresses and the second term (F^{NL}) the redistribution due to out-of-plane displacements. The coefficients f_{ij} are found by substituting $F(x,y)$, w and w_0 into the nonlinear plate compatibility equation, Eq. (6), and are given in Appendix A.

5. Load and response propagation

Any loading history can be approximated by a series of piecewise linear load paths (intervals) through a set of specified (reference) load stages (points) [9,6]. Present computations are restricted to proportional loading that can be expressed by

$$S_i(\Lambda) = \Lambda S_{i0}, \tag{12}$$

where $i = x, y, xy$. S_{i0} is an applied reference component and Λ is a load parameter with values between 0 and 1.

In load control analyses, Λ is specified and the corresponding displacements are computed. In displacement or arc length control analyses, on the other hand, Λ will be a function of either a specified displacement or of an arc length along the equilibrium path. In the present paper, load–displacement histories are traced using the incremental procedure presented in Steen [9], in which an arc length parameter η is chosen as the propagation (incrementation) parameter. The arc length along the equilibrium curve is always increasing and may be considered a pseudo-time. It is therefore a most suitable propagation parameter.

A non-dimensional arc length increment parameter $\Delta\eta$ can be related to an increment $\Delta\Lambda$ in the load parameter as illustrated in Fig. 2. From geometrical considerations, the relation given by

$$\dot{\Lambda}^2 + \sum_{i=1}^{M}\sum_{j=1}^{N}\frac{\dot{a}_{ij}^2}{t^2} = 1 \tag{13}$$

is obtained as the increment size approaches zero. The plate thickness t is introduced in order to obtain dimensional consistency.

The load parameter Λ and displacement amplitudes a_{ij} are now functions of the arc length parameter η. For an increment $\Delta\eta$ from point "k" to "$k+1$" along the equilibrium curve, a Taylor series expansion gives

$$a_{ij}^{k+1} = a_{ij}^{k} + \dot{a}_{ij}^{k}\Delta\eta + \tfrac{1}{2}\ddot{a}_{ij}^{k}\Delta\eta^2 + \cdots, \tag{14}$$

$$\Lambda^{k+1} = \Lambda^{k} + \dot{\Lambda}^{k}\Delta\eta + \tfrac{1}{2}\ddot{\Lambda}^{k}\Delta\eta^2 + \cdots. \tag{15}$$

Above, the "dot" notation is introduced for partial differentiation with respect to η, e.g., $\dot{\Lambda} = \partial\Lambda/\partial\eta$, $\ddot{\Lambda} = \partial^2\Lambda/\partial\eta^2$, etc. In the present paper, second and higher order terms are neglected. The resulting first order expansion is an approximation that is usually called the Euler or Euler–Cauchy method. By introducing equilibrium corrections after each increment $\Delta\eta$, such as in Riks' arc length method [14], the accuracy of the method for a given number of increments would be improved. Alternatively, the second order terms in Eqs. (14) and (15) can readily be included [9] to improve accuracy. Based on computational comparisons, Byklum [15] concluded that computational gains are not likely to be achieved by retaining second order terms as compared to use of only first order terms in combination with smaller increments $\Delta\eta$. Still another alternative is the improved Euler method (Heun's method), which is a predictor–corrector method [16]. It was considered in the present work, but not implemented as significant computational gains (efficiency) were not expected compared to the standard Euler method with smaller increments.

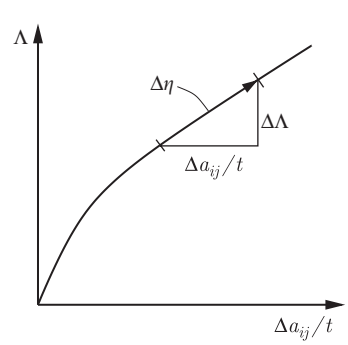

Fig. 2. Definition of the propagation parameter $\Delta\eta$ for a case with one amplitude a_{ij}.

6. Solution procedure

At a specific state "k" in the propagation process, the displacement rates ($\dot{a}_{ij}$) can be determined from the equilibrium equations on rate form and Eq. (13). The solution at state "$k+1$" can then be obtained as described above from

$$a_{ij}^{k+1} = a_{ij}^{k} + \dot{a}_{ij}^{k}\Delta\eta, \quad \Lambda^{k+1} = \Lambda^{k} + \dot{\Lambda}^{k}\Delta\eta. \tag{16}$$

According to the principle of stationary potential energy, equilibrium requires that the total potential energy $\Pi = U + T$, has a stationary value, i.e., $\delta\Pi = \delta U + \delta T = 0$. Here, U is the strain energy and T is the potential energy of the external loads. This requirement on rate form, $\delta\dot{\Pi} = \delta\dot{U} + \delta\dot{T} = 0$, leads to the $M \times N$ equations given by

$$\frac{\partial\dot{\Pi}}{\partial a_{fg}} = \frac{\partial\dot{U}_{\text{plate}}}{\partial a_{fg}} + \frac{\partial\dot{T}_{\text{plate}}}{\partial a_{fg}} + \frac{\partial\dot{U}_{\text{stiff}}}{\partial a_{fg}} + \frac{\partial\dot{T}_{\text{stiff}}}{\partial a_{fg}} = 0, \tag{17}$$

where $f = 1, 2, \ldots, M$ and $g = 1, 2, \ldots, N$. By grouping the various contributions, these $M \times N$ equations can be written as

$$\frac{\partial\dot{\Pi}}{\partial a_{fg}} = K_{fgpq}\dot{a}_{pq} + G_{fg}\dot{\Lambda} = 0, \tag{18}$$

where

$$K_{fgpq} = \frac{\partial^2\Pi}{\partial a_{fg}\partial a_{pq}} \quad \text{and} \quad G_{fg} = \frac{\partial^2\Pi}{\partial a_{fg}\partial\Lambda}. \tag{19}$$

Above, the index notation with the Einstein summation rule for repeated indexes is adopted. Alternatively, in the common matrix notation, the stationary potential energy on rate form can be written as

$$\mathbf{K}\dot{\mathbf{a}} + \mathbf{G}\dot{\Lambda} = \mathbf{0}, \tag{20}$$

where $\mathbf{K}$ is a generalised, incremental (tangential) stiffness matrix with dimension $(M \times N) \times (M \times N)$, $-\mathbf{G}\dot{\Lambda}$ is a

generalised, incremental load vector and $\dot{\mathbf{a}}$ is a displacement amplitude rate vector.

Eq. (18) (or (17)) represents $M \times N$ linear equations in the $M \times N + 1$ unknowns ($\dot{a}_{kl}$ and $\dot{\Lambda}$). Eq. (13) is the additional equation required. The solution of Eq. (18) is given by

$$\dot{a}_{pq} = \dot{\Lambda} K^{-1}_{fgpq} G_{fg} = \dot{\Lambda} d_{pq} \quad \text{where } d_{pq} = K^{-1}_{fgpq} G_{fg}. \tag{21}$$

By substituting Eq. (21) into Eq. (13), the following equation is obtained:

$$\dot{\Lambda}^2 \left(t^2 + \sum_{p=1}^{M} \sum_{q=1}^{N} d_{pq}^2 \right) = t^2 \tag{22}$$

from which the load rate parameter $\dot{\Lambda}$ can be determined as

$$\dot{\Lambda} = \pm \frac{t}{\sqrt{t^2 + \sum_{p=1}^{M} \sum_{q=1}^{N} d_{pq}^2}}. \tag{23}$$

There are two possible solutions with the same numerical value, but with opposite signs. One solution is in the direction of an increasing arc length and one in the opposite direction. The solution of interest corresponds to that giving a continuous increase of the arc length. This is assumed to be the solution which results in the smoothest equilibrium curve. In the same manner as in Steen [9], this is expressed by the requirement that the absolute value of the angle between the tangents of two consecutive states ("$k-1$" and "k") in the load–displacement ($\Lambda - a_{pd}/t$) space is smaller than 90°. Thus, for the correct sign of the load rate $\dot{\Lambda}^k$ at state "k", the following criterion must be satisfied:

$$\sum_{p=1}^{M} \sum_{q=1}^{N} \dot{\Lambda}^k \left(\frac{d_{pq}^k \dot{a}_{pq}^{k-1}}{t^2} + \dot{\Lambda}^{k-1} \right) > 0. \tag{24}$$

An equivalent criterion for choosing the correct sign is given in Byklum et al. [6].

When $\dot{\Lambda}^k$ at stage "k" is found, the displacement rate amplitudes $\dot{a}_{pq}^k$ are given by Eq. (21). The displacement amplitudes and load parameter at the next stage are then found from Eq. (16). In this manner, the solution propagation is continued until a specified limit, or given criterion, is reached. The present solution procedure is capable of passing limit points, including tracing of snap-through and snap-back equilibrium curves.

The advantage of using stationary potential energy on rate form is that it yields a set of linear equations in the unknown displacement rates. In comparison, by using the stationary of the potential energy directly, third order equations in a_{ij} result, because the total potential energy Π in large deflection theory is of fourth order in the amplitudes a_{ij}.

7. Potential energy of the plate and restraints

The potential strain energy of the plate and the potential energy of the external stress along the plate edges give contributions to the incremental stiffness matrix and the incremental load vector, respectively. The potential strain energy of the plate can be divided into a bending energy and membrane energy contribution, since the coupling term becomes zero when integrated over the plate thickness. The bending strain energy is of quadratic order in the displacement amplitudes and thereby gives a constant contribution to the incremental plate stiffness matrix (Eq. (18)) and, thus, needs to be calculated only once. The membrane energy is of fourth order in a_{ij} and its contribution to the incremental stiffness is of second order. Consequently, it must be computed for each new propagation increment. The plate's energy contributions on the rate form are given and discussed in more detail in Byklum [15] and Byklum et al. [6] and is not repeated here.

Both the out-of-plane displacements and the rotations along an arbitrary oriented line with length S may be restrained by applying translational and rotational springs, respectively. The strain energy due to such springs can readily be established [4]. Further details on energy rates for springs (obtained by differentiation) are not given here.

8. Potential energy of stiffeners

8.1. Sniped stiffeners

The stiffeners are modelled using beam theory in which the curvature of a stiffener is taken equal to the plate curvature in the direction of the stiffener ($w_{,ss}$) and in which the strain in a stiffener and the plate are equal at their intersection. These strains comply with moderately large deflection theory as reviewed previously. Fig. 3 illustrates how an eccentric stiffener of a plate in global bending tends to lift the axis of bending a distance $z = z_c$ above the middle plane of the plate. In a simplified manner, the stiffener strain ε_s to be used in energy calculations is assumed to have the distribution

$$\varepsilon_s(z) = \varepsilon_s^m - (z - z_c) w_{,ss}, \tag{25}$$

where ε_s^m is the plate membrane strain in the direction along the stiffener as computed without the shift-of-axis

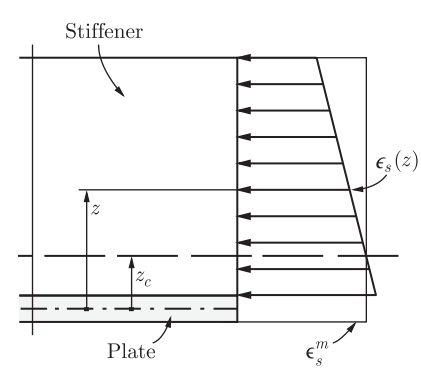

Fig. 3. Illustration of the strain distribution $\varepsilon_s(z)$ in an eccentric stiffener of plate in global bending.

effect. The shift of axis will also affect plate strains. However, integrated over the entire plate, the effect of a local shift of axis of bending on the plate strain energy is considered to be negligible.

The strain ε_s^m can be expressed in terms of the coordinate membrane strains from a regular strain transformation. Then, replacing the coordinate strains by coordinate stresses according to Hooke's law, and these stresses again by Airy's stress function (Eq. (9)), plate membrane strains ε_s^m can be expressed by

$$\varepsilon_s^m = \frac{1}{E}(k_x F_{,yy} + k_y F_{,xx} + k_{xy} F_{,xy}). \tag{26}$$

Here, $k_x = \cos^2\theta - \nu\sin^2\theta$, $k_y = \sin^2\theta - \nu\cos^2\theta$ and $k_{xy} = -(1+\nu)\sin 2\theta$. For a stiffener with length L_s and end coordinates (x_1, y_1) and (x_2, y_2), the angle between the x-axis and the stiffener becomes $\theta = \arccos((x_2 - x_1)/L_s)$. The strain ε_s^m in Eq. (26) consists of a linear contribution (due to F^L) and a nonlinear contribution (due to F^{NL}) due to the stress redistribution.

By substitution of Eq. (25) into the general strain energy expression, the strain energy of a stiffener with cross-section area A_s can be given by

$$\begin{aligned} U_{\text{stiff}} &= \frac{E}{2}\int_{L_s}\int_{A_s} \varepsilon_s^2 \,\mathrm{d}A_s\,\mathrm{d}L_s \\ &= \frac{E}{2}\int_{L_s}\int_{A_s}\Big((z-z_c)^2 w_{,ss}^2 - 2\varepsilon_s^m (z-z_c) w_{,ss} \\ &\quad + (\varepsilon_s^m)^2\Big)\mathrm{d}A_s\,\mathrm{d}L_s, \end{aligned} \tag{27}$$

where $w_{,ss}$ is the partial double derivative of w with respect to the direction along the stiffener. It can be obtained from the dot product between the unit direction vector $\mathbf{s} = (L_x\mathbf{i} + L_y\mathbf{j})/L_s$ in the direction of the stiffener and the gradient vectors $\nabla = \mathbf{i}\partial/\partial x + \mathbf{j}\partial/\partial y$ as

$$w_{,ss} = \nabla(\nabla w\cdot\mathbf{s})\cdot\mathbf{s} = \frac{1}{L_s^2}(L_x^2 w_{,xx} + 2L_x L_y w_{,xy} + L_y^2 w_{,yy}), \tag{28}$$

where $L_x = (x_2 - x_1)$ and $L_y = (y_2 - y_1)$. The strain energy integral may be solved analytically or by numerical integration. The latter is chosen in this paper.

For plates, the quadratic membrane strain term in the strain energy gives rise to a postbuckling reserve strength due to stress redistribution of the in-plane stresses. Such a stress redistribution is not possible for beams (stiffeners), and their postcritical reserve strength is much smaller. Consequently, the contribution of the quadratic ε_s^m term in Eq. (27) is rather small. In addition, this contribution is computationally rather expensive when the number of terms in the assumed Airy's stress function (Eq. (11)) is large, and it is conservatively neglected in the present model. Thus, the adopted strain energy expression of a stiffener becomes

$$U_{\text{stiff}} = \frac{EI_e}{2}\int_{L_s} w_{,ss}^2\,\mathrm{d}L_s - e_c E A_s \int_{L_s} w_{,ss}\varepsilon_s^m\,\mathrm{d}L_s, \tag{29}$$

where $e_c = z_{sc} - z_c$ is the distance from the axis of bending (at $z = z_c$) to the centre of the stiffener area (at $z = z_{sc}$) and I_e is the effective moment of inertia. The rate form of the contribution of the potential stiffener strain energy is given in Appendix A.

For eccentric stiffeners, the shift of the axis of bending brings in a contribution also from the plate. In order to account for this, I_e can be given by

$$I_e = \int_{A_s}(z - z_c)^2\,\mathrm{d}A_s + t b_e z_c^2, \tag{30}$$

where z_c is the distance from the middle plane of the plate to the centroidal axis (through the centre of area) of a cross-section consisting of the stiffener and a portion of the plate with an effective width b_e. The moment of inertia of the effective plate width about its own axis is not included in I_e as it is included in the energy of the plate itself. For a symmetric stiffener, $z_c = 0$ in Eq. (30). Also for eccentric stiffeners, use of $z_c = 0$ (for an infinite b_e) represents a reasonable simplification in many cases. Nevertheless, use of $z_c = 0$ may give somewhat non-conservative results for eccentric stiffeners in some cases. Possibly, b_e should not be taken greater than about $20t$ in practical design work [4].

The torsional stiffness of the stiffeners may be accounted for by including the torsional energy contribution. This is essential in conjunction with torsionally stiff, closed stiffener profiles. In the open stiffener profile examples of the present paper, the torsional stiffener stiffness is neglected. This is normally acceptable for such profiles.

8.2. Continuous stiffeners

Continuous stiffeners can be included in the model formulation by including the potential energy of the external stiffener loads. For stiffeners oriented in the x-direction, the resultant force acting on the two ends of a stiffener is equal if the bending modes are symmetric or asymmetric about $y = b/2$. For such cases, which are the most common cases, the potential energy of the external loads on one stiffener is taken according to

$$T_{\text{stiff}} = -P_{sx}\Delta_{sx} - P_{sx}e_c w_{2,x} + P_{sx}e_c w_{1,x}, \tag{31}$$

where $P_{sx} = -A_s\sigma_x^m = -A_s F_{,yy}$ is the resultant force (positive in compression) acting on the stiffener. The corresponding rotations at end 1 and end 2 are $w_{1,x}$ and $w_{2,x}$, respectively. For a plate subjected to constant external stress distributions, Δ_{sx} is taken as the plate shortening given by

$$\Delta_{sx} = -\int_0^L u_{,x}\,\mathrm{d}x = -\int_0^L\left(\varepsilon_x^m - \frac{1}{2}w_{,x}^2 - w_{0,x}w_{,x}\right)\mathrm{d}x \tag{32}$$

or following integration by

$$\Delta_{sx} = \Lambda\left(\frac{S_{x0}L}{E} - \nu\frac{S_{y0}L}{E}\right) + \frac{\pi^2}{8L}\sum_{i=1}^{M}\sum_{j=1}^{N} i^2(a_{ij}^2 + 2a_{ij}b_{ij}). \tag{33}$$

This shortening is independent of y. The two last terms in Eq. (31) are due to the rotation of the stiffener about the y-axis at the stiffener ends. The rate form of the contribution of Eq. (31) is given in Appendix A.

Eq. (31) is similar to, but more general than, an expression for potential energy of external stiffener loads given by Steen [17], who considered a plate with only one degree of freedom and with stiffener bending about the plate plane ($z_c = 0$).

For the local bending cases, which is of most practical interest, the stiffeners will remain nearly straight and only contribute negligibly to the total external energy. Then it makes little difference whether the stiffeners are sniped or continuous. The difference in the resulting force is equal to the additional load carried by the continuous stiffeners in such cases.

9. Verification premises

The theory presented in this paper has been implemented into a Fortran 90 computer program, and computed results have been verified for a variety of plate and stiffener dimensions by comparisons with large displacement, finite element analyses using ANSYS [18] in which both plate and stiffeners were modelled using Shell93 elements. Only proportional loading is considered (linear load paths). The external stresses are constant along the plate edges. Results are presented for biaxially, in-plane loaded plates provided with eccentric, sniped stiffeners and with regular and irregular stiffener arrangements. The stiffeners extend from the plate in the positive z-direction. For verification purposes, the imperfection distribution is taken, except when noted otherwise, as the first eigenmode calculated by ANSYS and the present model, respectively. If not noted otherwise, a maximum imperfection amplitude $w_{0,\max} = 5\,\text{mm}$ in the positive z-direction is used. The elastic material properties are Young's modulus $E = 208\,000\,\text{MPa}$ and Poisson's ratio $\nu = 0.3$.

Two different types of analysis results are presented in the consecutive sections. First, load–displacement curves (equilibrium paths) are computed by the present model and ANSYS for elastic plates. Second, predicted ultimate strengths for a plate with a material yield strength $f_Y = 235\,\text{MPa}$ are compared with fully nonlinear ANSYS analysis. The ANSYS analyses are performed with a bilinear stress–strain relationship having the same material properties E, ν and f_Y as above, and additionally a hardening modulus $E_T = 1000\,\text{MPa}$.

The finite element model is supported in the out-of-plane direction along the edges of the plate, and the edges are forced to remain straight during deformation. The plate is also supported in the in-plane directions, just enough to prevent rigid body motions. Further, the ends of the sniped stiffeners are completely free and not loaded.

The number of degrees of freedom used in ANSYS is typically about 20 000, which is believed to ensure satisfactory results. A typical element mesh is shown later (Fig. 9). In comparison, 225 degrees of freedom (15×15) are used by the present model in all cases. A rather small value of $\Delta\eta = 0.01$ is used in the comparisons with ANSYS results.

10. Stiffener simplifications

The general strain energy expression of a stiffener (Eq. (27)), which is in accordance with the moderately large deflection theory assumptions, was simplified by neglecting the term involving the quadratic membrane strain $(\varepsilon_s^m)^2$. This simplification (to the safe side), leading to Eq. (29), greatly increases the computational efficiency as discussed previously.

Also the membrane strain ε_s^m in Eq. (29), can be computationally quite costly. As defined by Eq. (26), ε_s^m is a function of both a linear (F^L) and a nonlinear (F^{NL}) stress variation (Eqs. (10)–(11)). The linear part does not affect the computational time significantly. It is rather simple, and its contribution to the incremental strain energy needs to be calculated only once. The nonlinear part, on the other hand, is a function of the out-of-plane displacements through a series solution that may consist of many terms (Eq. (11)) and that needs to be calculated for each new increment in the solution propagation.

For a plate with a single, eccentric stiffener considered below, the effect of neglecting the nonlinear part (F^{NL}) was to reduce the computational time, for a given number of increments, by a factor of about 30. In cases with multiple stiffeners, the difference in computational time may increase significantly.

It is consequently of considerable interest to establish whether the nonlinear F^{NL} part can be neglected or not. Although not of much importance from a computational time point of view, it is also of interest to study the effect of neglecting the membrane strain altogether, for instance by taking $F = 0$ or by neglecting the second term in the energy expression Eq. (29). This would give correct results for symmetric stiffeners (with $e_c = 0$). For eccentric stiffeners, this simplification implies that the stiffener is treated as a symmetric stiffener with an equivalent bending stiffness.

The various cases considered are listed below:

(a) ε_s^m computed with $F = F^L + F^{NL}$ and $b_e = 30t$.
(b) ε_s^m computed with $F = F^L$ and $b_e = 30t$.
(c) ε_s^m computed with $F = F^L$ and $z_c = 0$.
(d) $\varepsilon_s^m = 0$ (e.g., computed with $F = 0$) and $b_e = 30t$.

The case studied is a quadratic, simply supported plate that is provided with an eccentric, sniped stiffener with a flat bar profile. The stiffener is oriented along the middle of the plate. The plate is subjected to a constant uniaxial external stress in the stiffener direction. The maximum value of both the additional out-of-plane displacement and the imperfection is located in the centre of the plate. Thus, the total displacement mode is global.

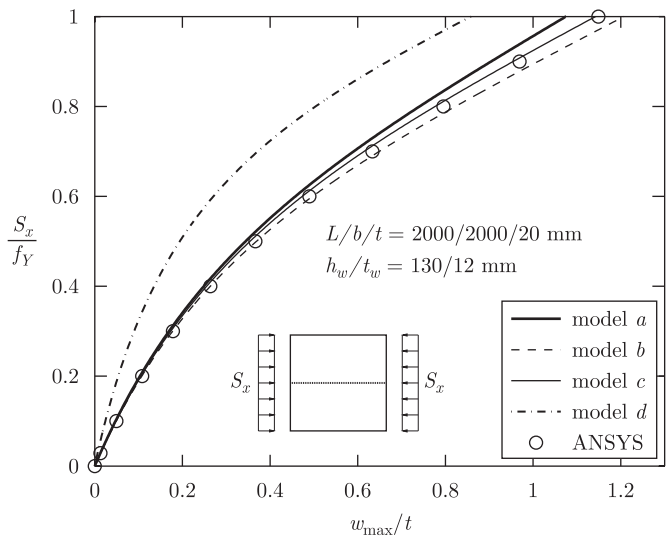

Fig. 4. Global load–displacement curves of a uniaxially loaded plate with an eccentric, flat bar stiffener—comparisons of results by ANSYS and the present model with different stiffener simplifications.

Fig. 4 shows load–displacement curves for the different stiffener modelling approaches. The figure also shows the results computed by ANSYS (open dots). The "complete" model "a" (thick, full line) is in good agreement with ANSYS, but slightly to the non-conservative side. However, the difference is rather small and is considered to be acceptable.

The effect of neglecting the nonlinear F^{NL} part can be seen by comparing curves "a" (thick line) and "b" (dashed line). It is seen to be conservative in this case, since its neglect results in a reduced plate stiffness and thereby larger displacements for given loads. The reason for this result can be discussed with reference to the last term of Eq. (29). In the present case with global bending in the positive z-direction, both ε_s^m (compression) and $w_{,ss}$ are negative. Thus, the last term in Eq. (29) reduces the stiffener energy and stiffness. This reduction is greatest when F^{NL} is neglected, since, at the stiffener location at the middle of the plate, the redistribution of stresses caused by F^{NL} (out-of-plane bending), tends to reduce the compression value of ε_s^m. If the global imperfection shape had been added in the negative z-direction, results of similar comparisons would be reversed. However, this case is rather academic, as imperfections to the same side as the eccentric stiffeners are in total more unfavourable, as will be shown later.

In global bending cases with more than one stiffener, the stress redistribution (F^{NL} effects) may result in additional compressive stresses in stiffeners close to the edges, and reduced compressive stresses in the stiffeners near the middle of the plate. Thus, the neglect of increased compression in some stiffeners is partly compensated for by reduced compressive stresses in other stiffeners. In conclusion, it is usually acceptable to neglect F^{NL} also in such cases.

The effect of calculating the strain energy with $z_c = 0$ ($b_e =$ "∞"), rather than with the more conservative value $b_e = 30t$, can be seen by comparing curve "c" (thin, full line) with curve "b" in Fig. 4. The difference between the two curves is rather small in this case with only one stiffener.

In cases with local bending, the curvature of the stiffeners will be small and thereby the strain energy contribution of the stiffeners will be small. Thus, in such cases, it is always a reasonable simplification to neglect the nonlinear contribution in the Airy's stress function. Moreover, it is also acceptable to include only the first integral in Eq. (29) in such cases. The latter simplification was used by Paik et al. [8] where it is stated that the effect of eccentricity is not studied in detail. However, this simplification is not recommended for the present, eccentrically stiffened plate in global bending, as seen by curve "d" in the figure. It is very non-conservative compared to the other curves.

11. Asymmetric bending behaviour

To demonstrate the ability of the present model to handle the effect of eccentric stiffeners, the plate with one eccentric, regular stiffener, described in Section 10 ($h_w/t_w = 130/12$ mm), and in addition the same plate with a weaker stiffener ($h_w/t_w = 100/12$ mm), are analysed. The plates are subjected to a uniaxial stress in the stiffener direction. It was found in the previous section that the displacement mode of the plate with the strongest stiffener is global, and thereby this is also the case for the other plate. For each plate, two different imperfections are studied, one added in the positive z-direction ($w_{0,\max} = 5$ mm) and one in the negative z-direction ($w_{0,\max} = -5$ mm).

Fig. 5 shows the load–displacement curves calculated with the stiffener modelling approach "a" (thick line) and "b" (dashed line), and by ANSYS (open dots). In the figure, w_{m} and $w_{0,\mathrm{m}}$ are the additional and initial displacement in the middle of the plate, respectively. The asymmetry in the shape of the load–displacement paths computed with positive and negative imperfections is due to the eccentric stiffener (in positive z-direction). The agreement between both modelling approaches and the ANSYS results is good.

The elastic buckling stress limit (ESL) is also shown in the figure (dash-dotted line). When the load–displacement paths approach this stress, the displacements increase more rapidly. For large displacements, the membrane stresses in the plate become more important and will tend to stabilise (stiffen) the response. This can be seen in Fig. 5(a).

Similar results for a plate provided with five regular stiffeners are shown in Fig. 6. The bending mode of the plate is global also in this case. Three different maximum imperfection amplitudes are studied ($w_{0,\max}/t = -0.5$, -0.25 and 0.25). The results by the present models are again in close agreement with the ANSYS results. Fig. 7 shows the total displacements along $x = L/2$, at the load $S_x = f_Y$, for the plate with a maximum initial imperfection case $w_{0,\max}/t = 0.25$. The overall out-of-plane displacement mode is clearly global.

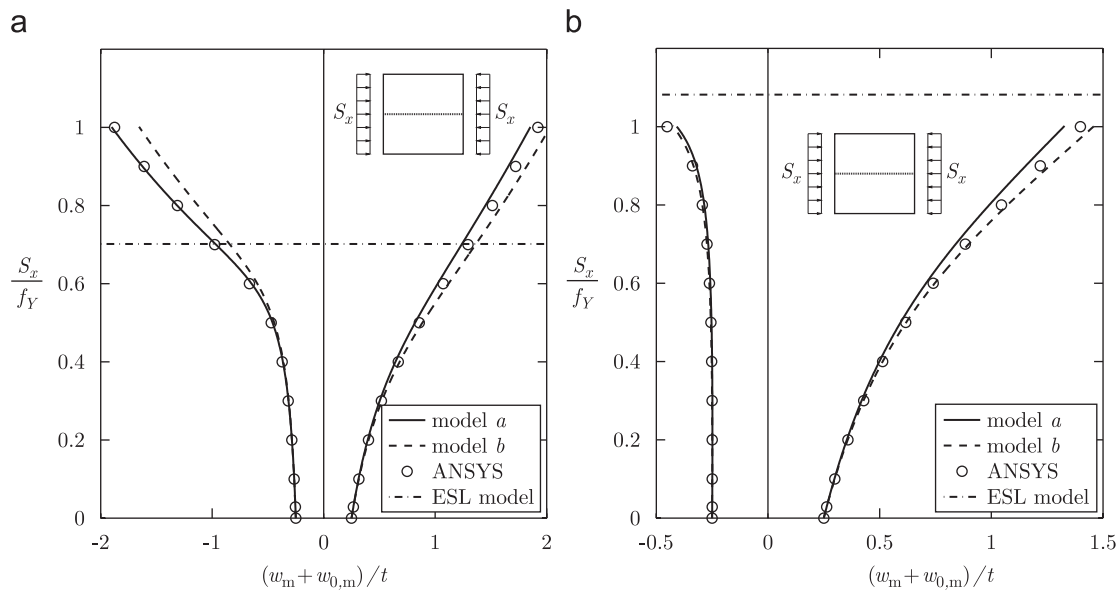

Fig. 5. Equilibrium paths of a uniaxially loaded plate ($L/b/t = 2000/2000/20$ mm) with one regular, flat bar stiffener with dimensions: (a) $h_w/t_w = 100/12$ mm and (b) $h_w/t_w = 130/12$ mm.

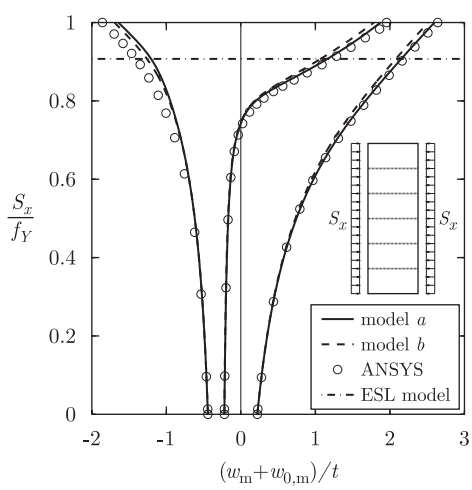

Fig. 6. Equilibrium paths of a uniaxially loaded plate ($L/b/t = 2000/6000/20$ mm) with five regular, flat bar stiffeners (dimensions $h_w/t_w = 130/12$ mm).

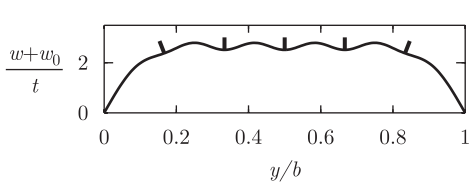

Fig. 7. Displacement profile along $x = L/2$ for $S_x/f_Y = 1$ of a regular, multi-stiffened plate with $w_{0,\max}/t = 0.25$ mm.

The middle set of curves in Fig. 6 is of particular interest. In this case, the effect of the negative imperfection amplitude $w_{0,\max}/t = -0.25$ is not large enough to overcome the effect of the eccentricity of the external loading (applied to the plate edges only). The corresponding total displacement curves cross-over from the negative side to the positive side at some load stage. For plates with continuous stiffeners, with external stresses applied to both plate and stiffeners, such "cross-overs" will not occur.

In practical design, the most conservative imperfection, which is that in the positive z-direction, is usually used. Further, for local bending cases, it does not affect the results significantly whether the imperfection is added in the positive or negative z-direction.

12. Irregularly stiffened plates

Plates with irregular stiffeners and a variety of plate and stiffener dimensions have been analysed. A typical case is shown in Fig. 8(a). The plate ($L/b/t = 1000/3000/10$ mm) is simply supported and is provided with two inclined, sniped stiffeners with a T-section ($h_w/t_w/b_f/t_f = 205/8/100/10$ mm). The rather irregular stiffener arrangement should provide a rather severe test case.

In the analysis, the stiffener modelling approach "a" described in Section 10 is used. The non-dimensional load-shortening curves calculated by the present model (thick, full line) for two uniaxial and one biaxial load case shown in Fig. 8(b), (c) and (d), respectively, are seen to be in good agreement with the ANSYS results (open dots). The curves are arbitrarily terminated at about $S_x = f_Y$. In the figure, the end shortenings Δ_x is in the x-direction, Δ_y is in the y-direction and $\varepsilon_Y = f_Y/E$ is the yield strain ($= 0.00113$). The elastic buckling stress limits (ESL) are also shown (dash-dotted lines). When the plate response curves exceed this stress, it can be seen that the plate stiffness is reduced.

The imperfection shapes, taken equal to the respective first buckling modes, are local in these cases. The total displacement mode ($w_0 + w$) remains local for increasing

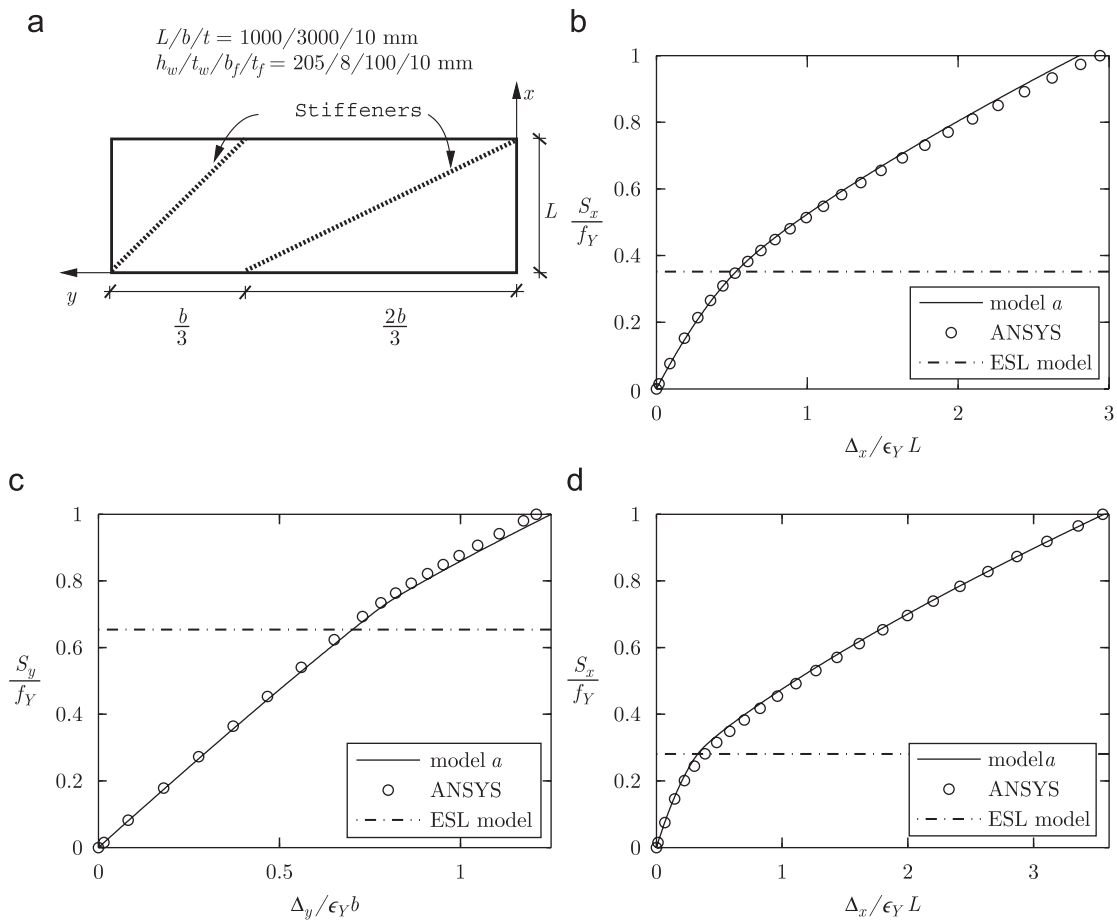

Fig. 8. (a) Overview of a plate with two inclined stiffeners, and load-shortening curves of the plate subject to (b) uniaxial loading in x-direction, (c) uniaxial loading in y-direction, and (d) biaxial loading ($S_x = S_y$).

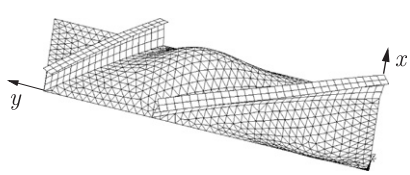

Fig. 9. The bending mode (by ANSYS) of the irregularly stiffened plate in Fig. 8(a) subjected to a biaxial loading $S_x = S_y = f_Y$.

loading. This can be seen in Fig. 9. For such cases, results will not be significantly affected if equal, but opposite imperfections, had been used. Further, for local bending cases, it makes little difference which of the stiffener modelling approaches (discussed in Section 10) that are used in the calculations.

13. Strength predictions

The ultimate strength limit of a plate, here shortened USL, is obtained when the limit point (maximum point) of the load–displacement curve is reached, i.e., when the curve starts to drop caused by an instability. Whereas a fully nonlinear finite element analysis, such as ANSYS, is able to predict such limit points, semi-analytical procedures of the kind presented here, is capable, when used in combination with a suitable "collapse" criterion, of predicting approximate USL loads. In such contexts, the von Mises' first yield criterion (i.e., $\sigma_e = f_Y$) is probably the most commonly used criterion. The equivalent stress ($\sigma_e = (\sigma_x^2 + \sigma_y^2 - \sigma_x\sigma_y + 3\tau_{xy}^2)^{1/2}$) in this criterion is sometimes computed at an outer plate surface [6], or taken equal to the membrane stress [4,5,15].

The applicability of this criterion applied to the membrane stresses in plates with irregular stiffeners is considered in this section. The critical points at which the von Mises' membrane stress reaches first yield are typically located in the plate along the edges and along the stiffeners. By using membrane stresses, rather than stresses in the outer fibres of the plate, some allowance is made for the additional section strength that can be developed after yielding in the outer fibres and for the stress redistribution caused by plasticity.

USL predictions by the present method (thick, full line) and by ANSYS (filled dots) are presented in Fig. 10 for the plate provided with two irregular stiffeners described in Section 12. Both biaxial compression–compression and compression–tension load combinations are included. No shear is applied. Also shown in the figure are elastic

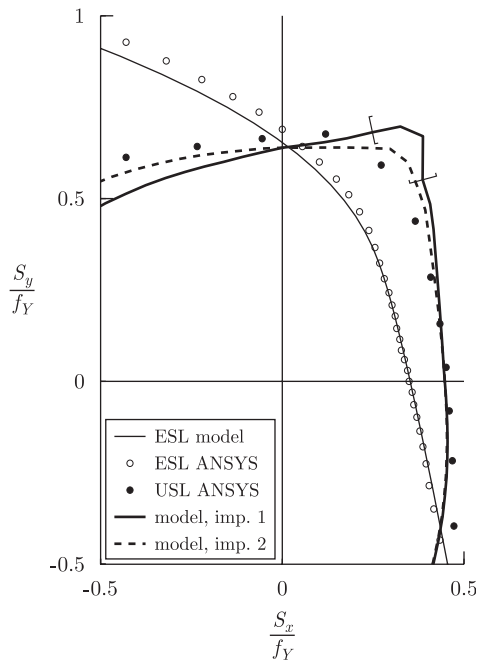

Fig. 10. Interaction curves in the stress space $S_x - S_y$ for the plate with irregular stiffener arrangement, described in Section 12.

buckling stress limits (ESL), or eigenvalues, calculated by the present model (thin, full curve) and by ANSYS (open dots). The agreement between the two ESL curves is very good. As mentioned previously (Verification premises), the corresponding first buckling modes, which are all local modes, are used as imperfections in the respective USL predictions for a given combination of S_x and S_y. The dashed USL results are based on another imperfection and will be discussed later.

By comparing ESL and USL results, it can be seen that the plate has a considerably reserve (postcritical) strength beyond the elastic buckling limit in the first quadrant (compression–compression combinations). This is typical for slender (thin) plates.

The USL predictions by the present model compare well with the fully nonlinear ANSYS results for a wide range of biaxial load combinations. The agreement is particularly good for cases with dominant compression in either the x- or y-direction. It is least good, and non-conservative, in cases with substantial compression in both directions, such as in the area with the "nose", between about $S_x = 0.70S_y$ and $S_x = 0.36S_y$, indicated by the square brackets in the figure.

In the region with the greatest discrepancy, the first few elastic buckling stress (ESL) values are probably quite close to each other, and other buckling modes than the first mode might possibly represent a more unfavourable imperfection. To investigate this, two additional imperfection shapes, corresponding to the elastic buckling modes obtained with uniaxial compression in the x- and y-direction, respectively, are considered. USL predictions by the present model have been obtained for both of these imperfections, and the lowest of the resulting values for each load combination is shown in Fig. 10 by the dashed line. These USL results compare much better with the ANSYS results than the previous (full, thick curve) ones.

Ultimate strength predictions by the present model clearly appear to be very sensitive to different imperfection assumptions. This might be especially true for such a slender plate as in this case study. The same is not the case with ANSYS predictions. Results based on the first buckling mode as well as on the two other modes discussed above have been obtained and are found to be very close. The reason for this might be that the development of plasticity in the ANSYS model possibly facilitates a smooth change in out-of-plane displacement shape to the most unfavourable shape almost irrespective of which of the three imperfection shapes that are used.

Due to the imperfection sensitivity of the present model, it seems recommendable to base the USL prediction, for a given load combination, on the lowest of the values obtained with imperfection shapes based on the first few (2–3) buckling modes. With appropriate simplifications in the stiffener modelling, as discussed previously, the method will still be computational efficient.

Based on the results above, von Mises' first yield criterion applied to membrane stresses seems like an acceptable strength criterion. Similar agreement has also been found by others [15]. It is emphasised, however, that all the plates referred to above had local out-of-plane displacement (buckling, postbuckling) shapes. This is in practise the most relevant case. For thicker plates and for stiffened plates in global bending, for which bending stresses become more important, indications are that a membrane stress criterion may not be sufficiently conservative in all cases. Membrane-bending stress interaction criteria, criteria related to stress limitations in the stiffener, etc., are possible topics for further study.

14. Step size and computational efficiency

In computations by the present model, the physical step size along the equilibrium path is dependent on the chosen propagation parameter value $\Delta\eta$ and the chosen size of the load interval, which is here equal to the chosen reference values S_{x0}, etc. The maximum reference value is taken equal to 1.5 f_Y. This is sufficiently large to allow the maximum membrane stress to reach von Mises' yield criterion in strength computations.

The influence of the step size $\Delta\eta$ on the accuracy of ultimate strength predictions is presented in Fig. 11. In the calculations, the nonlinear term in the Airy's stress function is neglected in the stiffener formulation ($F = F^L$). The inverse of the propagation parameter ($1/\Delta\eta$) gives an indication of how many increments that are used in a calculation. In the figure, the ultimate strengths are plotted relative to a ultimate strength $S_{x,250}$ predicted with a very small value of $\Delta\eta = 0.004$ ($1/\Delta\eta = 250$). In the results presented previously,

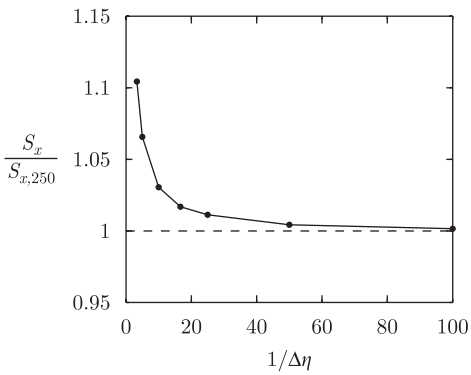

Fig. 11. Strength versus $\Delta\eta^{-1}$ for the irregularly stiffened plate in Fig. 8(a). Subjected to uniaxial loading S_x.

$\Delta\eta = 0.01$ ($1/\Delta\eta = 100$) was used, and from the figure, it is clear that the strength predictions have converged for this value.

Larger propagation parameter values can be justified in order to reduce the computation time. The calculated strength with $\Delta\eta = 0.04$ is only about 1.1% larger than $S_{x,250}$, which is clearly acceptable in practical design. For a given loading and given premises ($M \times N = 15 \times 15$, $\Delta\eta = 0.04$), the CPU time for a strength prediction using the computer program, which has not yet been optimised with regard to speed, is typically 7–8 s on a medium fast computer (1.5 GHz processor, 512 MB RAM memory). In comparison, the CPU time for the same case with $\Delta\eta = 0.004$ is about 60 s.

For irregular stiffener cases, it has been found that predicted ultimate strength results may be up to 6–7% greater than those that would have been obtained with two to three times the number of terms in each direction in the assumed displacement solution (Eq. (8)). If a convergence test is not carried out in a practical design situation, it would be appropriate to reduce the predicted strength by an amount of this order.

15. Concluding remarks

An efficient computational model for large deflection analysis of plates with arbitrary stiffener orientations has been presented and verified by comparison with finite element analysis results using ANSYS. The model is able to trace the plate response beyond the elastic buckling load. It is able to capture both local and global displacement modes as well as the asymmetric global bending behaviour of plates with eccentric stiffeners.

The accuracy and computational efficiency of different stiffener modelling approaches have been considered. It was found that by neglecting the nonlinear part (F^{NL}) of Airy's stress function ($F = F^L + F^{NL}$) in the stiffener strain expression, the computation time is reduced by more than a factor of 30. The linearised stiffener strain approximation gives sufficient accuracy and is a conservative approximation in most practical cases.

Ultimate strengths were predicted by the present method using von Mises' yield criterion to the membrane stresses. This criterion may be somewhat non-conservative for thick plates and plates in global bending, in which cases the bending stress becomes more important. Alternative criteria for such cases are possible topics for further study.

Ultimate strengths predictions by the present model may be very sensitive to different imperfection shapes. In such cases, strength analysis may be performed with various imperfection shapes in order to account for the more unfavourable imperfection.

Due to the computational efficiency of the present model, it is also suited for design optimisation and reliability studies that normally require large number of case studies.

Acknowledgements

The authors would like to thank dr.scient. Eivind Steen and dr.ing. Eirik Byklum, both at Det Norske Veritas (DNV), Norway, for their support and valuable discussions throughout the study. Special thanks goes to Eirik Byklum for making a nonlinear postbuckling program (in Fortran 90) for unstiffened plates available for use in this study. The computer program based on the theory in the present paper represents an extension of that buckling program.

Appendix A

A.1. Coefficients in Airy's stress function

The coefficients in Airy's stress function are

$$f_{ij} = \frac{E}{4(i^2 b/L + j^2 L/b)^2} \times \sum_{r=1}^{M}\sum_{s=1}^{N}\sum_{p=1}^{M}\sum_{q=1}^{N} c_{rspq}(a_{rs}a_{pq} + a_{rs}b_{pq} + a_{pq}b_{rs}), \quad (A.1)$$

where b_{pq} are the amplitudes of w_0, f_{00} is zero, and c_{rspq} are integer numbers given by

$$c_{rspq} = rspq + r^2q^2 \quad (A.2)$$

if $\pm(r-p) = i$ and $s+q = j$, or $r+p = i$ and $\pm(s-q) = j$, or

$$c_{rspq} = rspq - r^2q^2 \quad (A.3)$$

if $r+p = i$ and $s+q = j$, or $\pm(r-p) = i$ and $\pm(s-q) = j$, or

$$c_{rspq} = 0 \quad (A.4)$$

for other cases. More details of the derivation of the coefficients f_{ij} can be found in the literature [15]. In the derivation of the rate form of the stationary potential

energy the following derivatives of f_{ij} are involved:

$$\frac{\partial f_{ij}}{\partial a_{fg}} = \frac{E}{4(i^2b/L + j^2L/b)^2} \times \sum_{r=1}^{M}\sum_{s=1}^{N}(c_{fgrs} + c_{rsfg})(a_{rs} + b_{rs}), \tag{A.5}$$

$$\dot{f}_{ij} = \frac{E}{4(i^2b/L + j^2L/b)^2} \times \sum_{r=1}^{M}\sum_{s=1}^{N}\sum_{p=1}^{M}\sum_{q=1}^{N}(c_{pqrs} + c_{rspq})(a_{rs} + b_{rs})\dot{a}_{pq}, \tag{A.6}$$

$$\frac{\partial \dot{f}_{ij}}{\partial a_{fg}} = \frac{E}{4(i^2b/L + j^2L/b)^2}\sum_{p=1}^{M}\sum_{q=1}^{N}(c_{fgpq} + c_{pqfg})\dot{a}_{pq}. \tag{A.7}$$

A.2. Incremental potential strain energy of a stiffener

By substitution of the assumed displacement field, the potential strain energy of a stiffener given in Eq. (29) can be written as

$$\begin{aligned} U_{\text{stiff}} = &\sum_{i=1}^{M}\sum_{j=1}^{N}\sum_{k=1}^{M}\sum_{l=1}^{N} a_{ij}a_{kl}Q_1(i,j,k,l) \\ &+ \sum_{i=1}^{M}\sum_{j=1}^{N}\sum_{m=0}^{2M}\sum_{n=0}^{2N} a_{ij}f_{mn}Q_2(i,j,m,n) \\ &+ \sum_{i=1}^{M}\sum_{j=1}^{N} a_{ij}Q_3(i,j,\Lambda), \end{aligned} \tag{A.8}$$

where

$$\begin{aligned} &Q_1(i,j,k,l) \\ &= \frac{EI_e}{2L_s^4}\int_{L_s}\left[\left(L_x^2\left(\frac{i\pi}{L}\right)^2 + L_y^2\left(\frac{j\pi}{b}\right)^2\right)\sin\left(\frac{i\pi}{L}x\right)\sin\left(\frac{j\pi}{b}y\right)\right. \\ &\quad \left.\frac{i\pi}{L} - 2L_xL_y\left(\frac{i\pi}{L}\right)\left(\frac{j\pi}{b}\right)\cos\left(\frac{i\pi}{L}x\right)\cos\left(\frac{j\pi}{b}y\right)\right] \\ &\quad \cdot\left[\left(L_x^2\left(\frac{k\pi}{L}\right)^2 + L_y^2\left(\frac{l\pi}{b}\right)^2\right)\sin\left(\frac{k\pi}{L}x\right)\sin\left(\frac{l\pi}{b}y\right)\right. \\ &\quad \left.\frac{k\pi}{L} - 2L_xL_y\left(\frac{k\pi}{L}\right)\left(\frac{l\pi}{b}\right)\cos\left(\frac{k\pi}{L}x\right)\cos\left(\frac{l\pi}{b}y\right)\right]\mathrm{d}L_s, \end{aligned} \tag{A.9}$$

$$\begin{aligned} &Q_2(i,j,m,n) \\ &= \frac{e_cA_s}{L_s^2}\int_{L_s}\left[\left(L_x^2\left(\frac{i\pi}{L}\right)^2 + L_y^2\left(\frac{j\pi}{b}\right)^2\right)\sin\left(\frac{i\pi}{L}x\right)\sin\left(\frac{j\pi}{b}y\right)\right. \\ &\quad \left.\frac{i\pi}{L} - 2L_xL_y\left(\frac{i\pi}{L}\right)\left(\frac{j\pi}{b}\right)\cos\left(\frac{i\pi}{L}x\right)\cos\left(\frac{j\pi}{b}y\right)\right] \\ &\quad \cdot\left[\left(k_x\left(\frac{n\pi}{b}\right)^2 + k_y\left(\frac{m\pi}{L}\right)^2\right)\cos\left(\frac{m\pi}{L}x\right)\cos\left(\frac{n\pi}{b}y\right)\right. \\ &\quad \left.-k_{xy}\left(\frac{n\pi}{L}\right)\left(\frac{m\pi}{L}\right)\sin\left(\frac{m\pi}{L}x\right)\sin\left(\frac{n\pi}{b}y\right)\right]\mathrm{d}L_s, \end{aligned} \tag{A.10}$$

$$\begin{aligned} Q_3(i,j,\Lambda) = &-\frac{\Lambda e_cA_s}{L_s^2}\int_{L_s}[k_xS_{0x}(y) + k_yS_{0y}(x) + k_{xy}S_{0xy}] \\ &\cdot\left[\left(L_x^2\left(\frac{i\pi}{L}\right)^2 + L_y^2\left(\frac{j\pi}{b}\right)^2\right)\sin\left(\frac{i\pi}{L}x\right)\sin\left(\frac{j\pi}{b}y\right)\right. \\ &\left.-2L_xL_y\left(\frac{i\pi}{L}\right)\left(\frac{j\pi}{b}\right)\cos\left(\frac{i\pi}{L}x\right)\cos\left(\frac{j\pi}{b}y\right)\right]\mathrm{d}L_s. \end{aligned} \tag{A.11}$$

The rate form of the contribution of the stiffener strain energy in the principle of stationary potential energy is

$$\begin{aligned} \frac{\partial \dot{U}_{\text{stiff}}}{\partial a_{fg}} &= \frac{\partial^2 U_{\text{stiff}}}{\partial a_{fg}\partial a_{pq}}\dot{a}_{pq} + \frac{\partial^2 U_{\text{stiff}}}{\partial a_{fg}\partial \Lambda}\dot{\Lambda} \\ &= \sum_{p=1}^{M}\sum_{q=1}^{N}(Q_1(p,q,f,g) + Q_1(f,g,p,q))\dot{a}_{pq} \\ &\quad + \sum_{m=0}^{2M}\sum_{n=0}^{2N}Q_2(f,g,m,n)\dot{f}_{mn} \\ &\quad + \sum_{p=1}^{M}\sum_{q=1}^{N}\sum_{m=0}^{2M}\sum_{n=0}^{2N}Q_2(p,q,m,n)\frac{\partial f_{mn}}{\partial a_{fg}}\dot{a}_{pq} \\ &\quad + \sum_{i=1}^{M}\sum_{j=1}^{N}\sum_{m=0}^{2M}\sum_{n=0}^{2N}Q_2(i,j,m,n)a_{ij}\frac{\partial \dot{f}_{mn}}{\partial a_{fg}} \\ &\quad + \dot{Q}_3(f,g,\Lambda), \end{aligned} \tag{A.12}$$

where the expressions $\dot{f}_{mn}$, $\partial f_{mn}/\partial a_{fg}$ and $\partial \dot{f}_{mn}/\partial a_{fg}$ are defined in Eqs. (A.5)–(A.7). The first four summation terms in Eq. (A.12) give contributions to the generalised, incremental stiffness matrix, while the last summation term gives a contribution to the generalised, incremental load vector.

A.3. Incremental potential energy of an external stiffener load

For a regular stiffener oriented in the x-direction, the rate form of the contribution of the potential energy due to external stiffener loads in the principle of stationary potential energy is

$$\begin{aligned} \frac{\partial \dot{T}_{\text{stiff}}}{\partial a_{fg}} &= \frac{\partial^2 T_{\text{stiff}}}{\partial a_{fg}\partial a_{pq}}\dot{a}_{pq} + \frac{\partial^2 T_{\text{stiff}}}{\partial a_{fg}\partial \Lambda}\dot{\Lambda} \\ &= \frac{\partial \dot{P}_{sx}}{\partial a_{fg}}\left(e_c[w_{,x}]_{(x_1,y_1)}^{(x_2,y_2)} - \Delta_x\right) + \frac{\partial P_{sx}}{\partial a_{fg}}\left(e_c[\dot{w}_{,x}]_{(x_1,y_1)}^{(x_2,y_2)} - \dot{\Delta}_x\right) \\ &\quad + \dot{P}_{sx}\left(e_c\frac{\partial}{\partial a_{fg}}[w_{,x}]_{(x_1,y_1)}^{(x_2,y_2)} - \frac{\partial \Delta_x}{\partial a_{fg}}\right) - P_{sx}\frac{\partial \dot{\Delta}_x}{\partial a_{fg}}, \end{aligned} \tag{A.13}$$

where

$$\frac{\partial \Delta_x}{\partial a_{fg}} = \frac{\pi^2}{4L}f^2(a_{fg} + b_{fg}), \tag{A.14}$$

$$\frac{\partial \dot{\Delta}_x}{\partial a_{fg}} = \frac{\pi^2}{4L}f^2\dot{a}_{fg}, \tag{A.15}$$

$$\dot{\Delta}_x = \dot{\Lambda}\left(\frac{S_{x0}L}{E} - \nu\frac{S_{y0}L}{E}\right) + \frac{\pi^2}{4L}\sum_{p=1}^{M}\sum_{q=1}^{N} p^2(a_{pq}+b_{pq})\dot{a}_{pq}, \tag{A.16}$$

$$\dot{w}_{,x} = \sum_{p=1}^{M}\sum_{q=1}^{N}\dot{a}_{pq}\frac{\pi p}{L}\,cos\left(\frac{\pi p x}{L}\right)\sin\left(\frac{\pi q y}{b}\right), \tag{A.17}$$

$$\frac{\partial P_{sx}}{\partial a_{fg}} = \sum_{m=0}^{2M}\sum_{n=0}^{2N}\frac{\partial f_{mn}}{\partial a_{fg}}\left(\frac{n\pi}{b}\right)^2\cos\left(\frac{m\pi}{L}x_2\right)\cos\left(\frac{n\pi}{b}y_2\right), \tag{A.18}$$

$$\dot{P}_{sx} = -\dot{\Lambda}S_{x0} + \sum_{m=0}^{2M}\sum_{n=0}^{2N}\dot{f}_{mn}\left(\frac{n\pi}{b}\right)^2\cos\left(\frac{m\pi}{L}x_2\right) \times\cos\left(\frac{n\pi}{b}y_2\right), \tag{A.19}$$

$$\frac{\partial\dot{P}_{sx}}{\partial a_{fg}} = \sum_{m=0}^{2M}\sum_{n=0}^{2N}\frac{\partial\dot{f}_{mn}}{\partial a_{fg}}\left(\frac{n\pi}{b}\right)^2\cos\left(\frac{m\pi}{L}x_2\right)\cos\left(\frac{n\pi}{b}y_2\right), \tag{A.20}$$

where the expressions $\dot{f}_{mn}$, $\partial f_{mn}/\partial a_{fg}$ and $\partial\dot{f}_{mn}/\partial a_{fg}$ are defined in Eqs. (A.5)–(A.7). The terms in Eq. (A.13) containing $\dot{a}_{pq}$ give contributions to the generalised, incremental stiffness matrix, while terms containing $\dot{\Lambda}$ give contributions to the generalised, incremental load vector.

References

[1] prEN 1993-1-5, Eurocode 3: design of steel structures. Part 1.5: plated structural elements. Brussels: CEN, European Committee for Standardisation; 2005.

[2] Det Norske Veritas. DNV Rules for classification of ships. Det Norske Veritas, Høvik, Norway, 2002.

[3] Det Norske Veritas. Recommended practice DNV-RP-C201, Buckling strength of plated structures, Høvik, Norway, 2002.

[4] Brubak L, Hellesland J, Steen E. Semi-analytical buckling strength analysis of plates with arbitrary stiffener arrangements. J Constr Steel Res 2007;63(4):532–43.

[5] Brubak L, Hellesland J. Approximate buckling strength analysis of arbitrarily stiffened, stepped plates. Eng Struct 2007;13 doi:10.1016/j.engstruct.2006.12.002.

[6] Byklum E, Amdahl J. A simplified method for elastic large deflection analysis of and stiffened panels due to local buckling. Thin-Walled Struct 2000;40(11):925–53.

[7] Byklum E, Steen E, Amdahl J. A semi-analytical model for global buckling and postbuckling analysis of stiffened panels. Thin-Walled Struct 2004;42(5):701–17.

[8] Paik JK, Lee MS. A semi-analytical method for the elastic–plastic large deflection analysis of stiffened panels under combined biaxial compression/tension, biaxial in-plate bending, edge shear, and lateral pressure loads. Thin-Walled Struct 2005;43(3):375–410.

[9] Steen E. Application of the perturbation method to plate buckling problems. Research Report in Mechanics, No. 98-1, Mechanics Division, Department of Mathematics, University of Oslo, Norway; 1998. 60pp.

[10] Bažant ZP, Cedolin L. Stability of structures. Oxford: Oxford University Press; 1991.

[11] Brush DO, Almroth BO. Buckling of bars plates and shells. New York: McGraw-Hill Book Company; 1975.

[12] Marguerre K. Zur theorie der gekrümmten platte grosser formänderung. In: Proceedings of the 5th international congress for applied mechanics, 1938. p. 93–101.

[13] Levy, S. Bending of rectangular plates with large deflections. Report 737, NACA, 1942.

[14] Riks E. An incremental approach to the solution of snapping and buckling problems. Int J Solids Struct 1979;15:529–51.

[15] Byklum E. Ultimate strength analysis of stiffened steel and aluminium panels using semi-analytical methods. Dr. Ing. thesis, Norwegian University of Science and Technology, Trondheim, Norway; 2002.

[16] Kreyszig E. Advanced engineering mathematics. 7th ed. New York: Wiley; 1993.

[17] Steen E. Elastic buckling and postbuckling of eccentrically stiffened plates. Int J Solids Struct 1989;25(7):751–68.

[18] ANSYS Inc., ANSYS Documentation 9.0, Southpointe, Canonsburg, PA; 2004.